J. Fluid Mech. (1970), *vol.* 43, *part* 4, *pp.* 801–811
Printed in Great Britain

The flat plate boundary layer. Part 1. Numerical integration of the Orr–Sommerfeld equation

By R. JORDINSON
Department of Mathematics (Applied), University of Edinburgh

(Received 6 August 1969 and in revised form 15 February 1970)

Numerical space-amplified solutions of the Orr–Sommerfeld equation for the case of a boundary layer on a flat plate have been calculated for a wide range of values of frequency and Reynolds number. The mean flow is assumed to be parallel and given by the appropriate component of the Blasius solution. The results are presented in a form suitable for comparison with experiment and are also compared with calculations of earlier authors.

Introduction

The initial stage of the transition process in the Blasius boundary layer on a flat plate is a problem which has received much attention in both theory and experiment. In this stage of the transition process interest is centred on the stability of small, two-dimensional periodic disturbances in the boundary layer. The theoretical model is usually taken to be the Orr–Sommerfeld differential equation, the solution to which reduces to an eigenvalue problem when the appropriate boundary conditions are applied. The analytical solutions have usually been calculated assuming that the disturbances are subject to amplification in time; in experiments, however, the disturbances are injected continuously and amplification in space is observed. Nevertheless, the agreement between theory and experiment is regarded as satisfactory especially when account is taken of Gaster's (1962, 1965) formulae for relating space and time amplification.

A need arose, however, to provide some more detailed solutions of the Orr–Sommerfeld equation for comparison with the results of new experiments on the Tollmien–Schlichting waves which were being carried out in the low-turbulence wind tunnel of the Department of Natural Philosophy, Edinburgh. It was considered that these solutions should be calculated for amplification in space and that, in order to match the wide range of experimental parameters involved, the solutions should be calculated on an electronic computer. These solutions form the basis of the work described in this paper. They employ a method originally developed by Osborne who used it to calculate a time-amplified solution to the problem. The differential equation is replaced by a finite-difference approximation and Osborne's iteration is used to calculate the eigenvalues.

The differential equation and form of the solutions

The flat plate is assumed to lie in the plane $z = 0$ with the leading edge coincident with the y axis. The equations of motion are made dimensionless using the dimensional constants U_0, the free stream velocity, δ_1, the displacement thickness of the Blasius boundary layer and ν, the kinematic viscosity.

The non-dimensional mean flow in the boundary layer, $U(z)$, is assumed to be parallel to the plate and given by the x component velocity of the Blasius solution. The two-dimensional perturbation is expressed in terms of the dimensionless stream function

$$\psi(x,z,t) = \phi(z)\, e^{i(\alpha x-\beta t)} = \phi(z)\, e^{i\alpha(x-ct)}, \tag{1}$$

where the parameters α, β and c represent, respectively, the wave-number, frequency and phase velocity of the perturbation. The amplitude of the perturbation is assumed to be small and the substitution of ψ in the non-dimensional linearized vorticity equation for the perturbation leads to the Orr–Sommerfeld equation

$$(i/R)\,(D^2-\alpha^2)^2\phi+(\alpha U-\beta)\,(D^2-\alpha^2)\,\phi-\alpha\phi D^2U = 0, \tag{2}$$

where $D = d/dz$ and $R = U_0\delta_1/\nu$. The boundary conditions follow from the fact that the perturbation velocities vanish at the wall and far out in the mainstream. The first condition leads immediately to

$$\phi = D\phi = 0 \quad \text{at} \quad z = 0. \tag{3}$$

For the outer boundary conditions we note that for large values of z, (2) takes the form

$$(i/R)\,(D^2-\alpha^2)^2\phi+(\alpha-\beta)\,(D^2-\alpha^2)\,\phi = 0. \tag{2a}$$

The required solution of (2a) which fits the outer boundary condition is evidently

$$\phi = A\, e^{-\alpha z}+B\, e^{-\gamma z},$$

where A and B are arbitrary constants, and $\gamma^2 = \alpha^2+iR(\alpha-\beta)$. For the values of α, β and R relevant to the problem it is evident that $|\gamma| \gg |\alpha|$ so that $|e^{-\alpha z}| \gg |e^{-\gamma z}|$ for $z > 0$. Hence the relevant condition can be expressed in the form

$$\phi \sim e^{-\alpha z} \tag{4}$$

for large values of z. In the analytical solutions this condition is applied at the edge of the boundary layer, but in the present calculations, following Kurtz (1961) and Osborne (1967), (4) is applied at $z = 6$.

It is well known that the solution of (2) with the boundary conditions (3) and (4) poses an eigenvalue problem. In the space-amplified case considered here it is assumed that β and R are real and given, and the problem is that of finding a complex eigenvalue α with a corresponding eigenvector ϕ. In the time-amplified calculations hitherto considered by most authors, the corresponding problem is that of finding a complex eigenvalue c (or β) for given, real values of R and α.

The direct calculations of α and ϕ do not give all the results required for comparison with experiment and more detailed results have been directly computed. Additional calculations of this kind were carried out, for example, by Schlichting (1935), Shen (1954 and private communication) and Osborne (1967). The present calculations include (i) the variation of α with β for several values of R; (ii) the loci α_i = constant in the β, R plane, where the locus $\alpha_i = 0$ is, of course,

the neutral curve; and (iii) the total amplification of a disturbance propagating downstream at constant frequency. In this case, following Shen (private communication), the curves are plotted in the form $\ln(A/A_0)$ *vs.* R for different values of the dimensionless frequency parameter $F = \beta/R = \beta_r' \nu/U_0^2$ where β_r' is the angular frequency of the oscillation. The appropriate formula is

$$\ln \frac{A}{A_0} = \frac{2}{m^2} \int_{R_0}^{R} (-\alpha_i)\, dR, \tag{5}$$

where m is the Blasius constant 1·7208, A is the amplitude of the disturbance at a point R, and A_0, R_0 represent the amplitude and Reynolds number respectively at a point on branch I of the neutral stability curve corresponding to the given value of F. Since $\beta = FR$ the lines $F =$ constant in the β, R plane appear as straight lines through the origin (see figure 3).

The numerical methods

The method developed by Osborne (1967) is in two parts. In the first part the differential equation is replaced by a set of difference equations which is referred to as the algebraic model. A transformation of Numerov (1924) type is applied to the function ϕ, the truncation errors in the expressions for $D^4\phi$ and $D^2\phi$ being thus reduced to $O(h^6)$ and $O(h^4)$ respectively, where h is the step length used in the numerical integration. The algebraic model can be expressed in matrix form and the second part of the numerical method uses an iterative technique to find the eigenvalues of the matrix. The iteration scheme is the same as that given in Osborne (1967) where it appears as a third-order process, but in the present calculations the iteration is second order. Osborne pointed out that the order of the iteration depends on the way in which the eigenvalue parameter appears in the governing equation. In his case the eigenvalue, c, appeared linearly, but in the space-amplification case α appears non-linearly. There is further discussion of this point in Osborne (1964).

A computer program was written in Atlas Autocode to perform the iteration, i.e. to find α_r and α_i for given real values of R and β. The starting values for the iteration were usually taken from the results given in Osborne's paper.

It is necessary to make a suitable choice of the step length h used in the calculations and h is, in practice, fixed by choosing the number n of equal intervals into which the range $0 \leqslant z \leqslant 6$ is subdivided, so that $h = 6/n$. Kurtz (1961) and Osborne (1967) used $n = 40$ and this choice of n was used in the first runs of the present calculations. The program was then adapted to work with arbitrary choice of n and runs were made taking $n = 40\,(20)\,100$ for a given R and β. Finally, it was decided to use $n = 80$ for the main calculation, this value representing the best compromise between the competing demands of accuracy on one hand and of machine storage space on the other. With $n = 80$, α_r appears to be accurate to the fifth decimal place and α_i to within 5 units in that place.

Further programs were written to give the calculated functions (ii) and (iii) of the previous section. These programs were similar to those used by Osborne (1967).

Results of the calculations

(i) α_r *and* α_i *as functions of* β *at constant* R

These results are shown in figures 1 and 2, drawn for values of R ranging from 400 to 3000. At each value of R the range of values of β was chosen to include the whole region of amplification and also sections of the damping region near the neutral curve. For amplification α_i must be negative and it is evident from

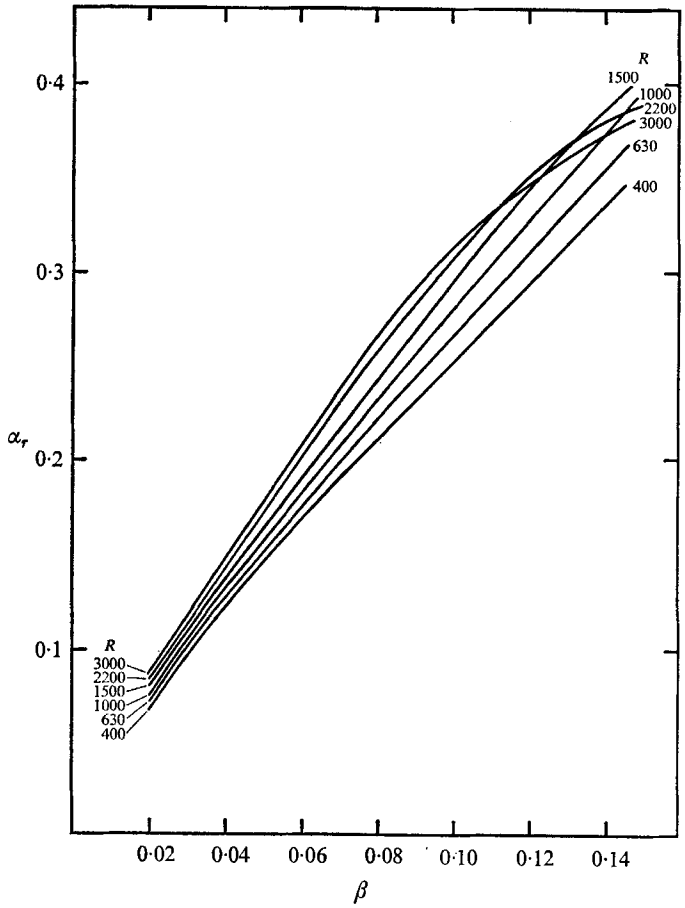

FIGURE 1. Variation of α_r with β at constant R.

figure 2 that, according to the present calculations, the critical Reynolds number is slightly greater than 500. In figure 1 the graphs of α_r *versus* β are almost straight lines and the slope of these lines representing the reciprocal of the group velocity (see Gaster 1965) becomes slightly steeper as the Reynolds number increases. It will be noticed however that there is a departure from this near linearity at values of β which correspond to points in the damping region adjacent to branch II of the neutral curve.

(ii) *Curves of constant amplification*

The curves of α_i = constant are shown in figure 3 and the important parameters of the neutral stability curve are given in table 1. The critical Reynolds number is 520, the corresponding value of β being 0·12. The numerical step-by-step calculations of Kaplan (1964) give a neutral stability curve which is almost identical

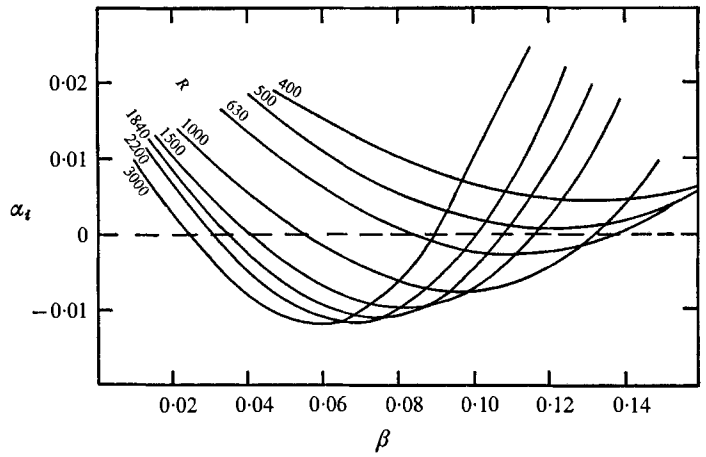

FIGURE 2. Variation of α_i with β at constant R.

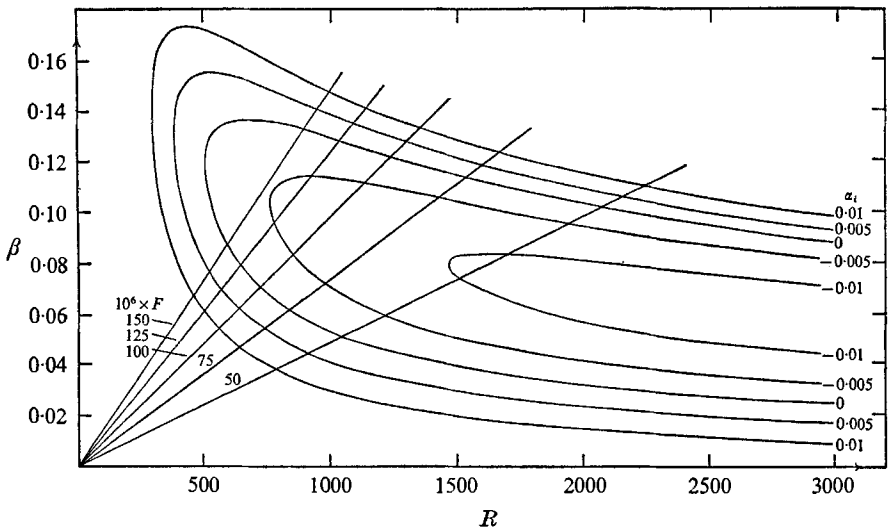

FIGURE 3. Curves of constant α_i.

with the present results. It has been noted by Obremski *et al.* (1969) that the various recent stability calculations carried out by different modern numerical methods have given remarkably consistent results. This is clearly exemplified by a comparison of the neutral stability curve of Wazzan *et al.* (1968) for the Blasius profile with the curve for $\alpha_i = 0$ in figure 3. The two

curves appear to be identical, and have exactly the same critical Reynolds number, 520.

The analytical solutions of Lin (1945) and Shen (1954), however, give a much lower critical Reynolds number of about 425, and a neutral stability curve which lies entirely outside the curve $\alpha_i = 0$ in figure 3. The maximum value of F on the neutral stability curve is 245×10^{-6} in the present work, and 345×10^{-6} according to Shen.

(iii) *Curves of total amplification*

The curves showing the growth of a disturbance propagating downstream at constant F, calculated from (5), are given in figure 4 (*a*) for $F \times 10^6 = 50\,(25)\,150$. Curves of this kind were calculated by Shen (private communication) using the time-amplification formula

$$\ln \frac{A}{A_0} = \frac{2}{m^2} \int_{R_0}^{R} \frac{\alpha c_i}{c_r + \alpha\, \partial c_r / \partial \alpha}\, dR. \tag{6}$$

R	α_r	β	$\partial\alpha_r/\partial\beta$	$\partial\alpha_i/\partial\beta$
3000	0·2878	0·0894	2·4899	0·7925
2600	0·2973	0·0947	2·4726	0·7501
2200	0·3084	0·1010	2·4495	0·6983
1800	0·3212	0·1088	2·4178	0·6326
1400	0·3359	0·1185	2·3721	0·5453
1000	0·3512	0·1306	2·2971	0·4153
800	0·3559	0·1368	2·2419	0·3197
600	0·3466	0·1380	2·1826	0·1724
531	0·3233	0·1293	2·1562	0·0570
520	0·3012	0·1193	2·1691	−0·0156
531	0·2806	0·1093	2·1949	−0·0738
559	0·2604	0·0993	2·2348	−0·1268
604	0·2405	0·0893	2·2892	−0·1784
671	0·2205	0·0793	2·3598	−0·2299
764	0·2011	0·0697	2·4510	−0·2826
964	0·1746	0·0568	2·6202	−0·3617
1164	0·1576	0·0489	2·7632	−0·4184
1364	0·1455	0·0433	2·8990	−0·4636
1764	0·1289	0·0360	3·1168	−0·5328
2164	0·1178	0·0313	3·3002	−0·5864
2564	0·1097	0·0280	3·4652	−0·6303
2964	0·1034	0·0255	3·6121	−0·6674

TABLE 1. Parameters on the neutral curve.

Figure 4 (*b*) shows a comparison between three of Shen's curves and the corresponding curves obtained in the present work. In general Shen's curves show greater amplification and it will be noticed that the positions of the turning values on each pair of curves in figure 4 (*b*) differ slightly. These turning values correspond to points on branch I and branch II of the neutral curve, so that this disagreement is consistent with the results of the comparison noted in the previous section where Shen's zone of amplification is larger than that in the present calculations.

(iv) *The eigenfunctions*

The iterative method used to find the eigenvalues also gives the corresponding eigenfunction, and the program for the basic iteration was adapted to print out its real and imaginary parts as functions of z for given values of R and β. Table 2 shows the values of $\mathrm{Re}\,\phi$ and $\mathrm{Im}\,\phi$ obtained in the present work for $R = 998$ and $\beta = 0{\cdot}1122$. In the table the eigenfunction has been normalized to make $\max \mathrm{Re}\,\phi = 1$.

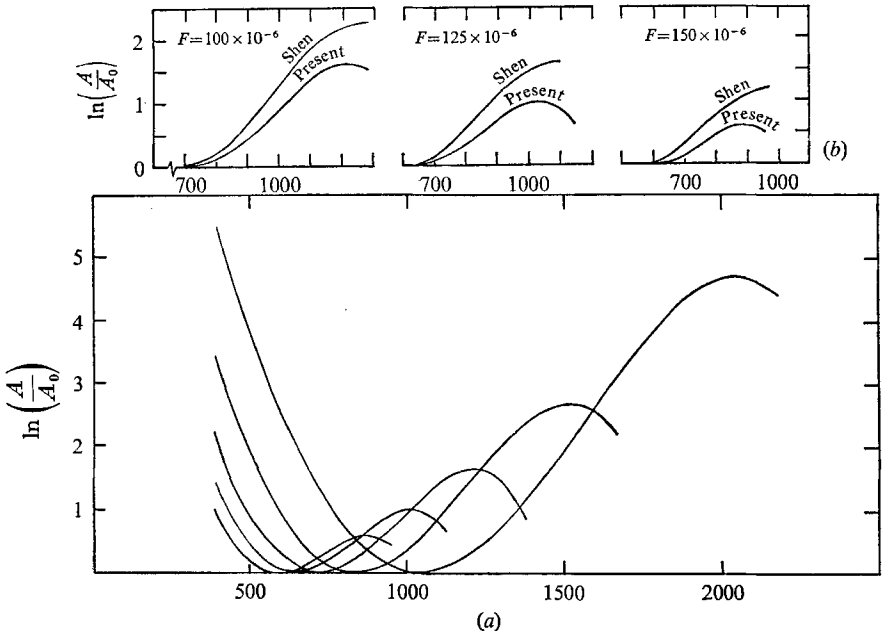

FIGURE 4. Curves of total amplification.

z	$\mathrm{Re}\,\phi$	$\mathrm{Im}\,\phi$	z	$\mathrm{Re}\,\phi$	$\mathrm{Im}\,\phi$
0	0	0	2·7	0·89272	0·00379
0·15	0·05296	−0·02852	3·0	0·82447	0·00466
0·3	0·16979	−0·05130	3·3	0·75568	0·00540
0·45	0·30310	−0·05076	3·6	0·69024	0·00603
0·6	0·43501	−0·03921	3·9	0·62961	0·00654
0·75	0·55890	−0·02728	4·2	0·57403	0·00693
0·9	0·66994	−0·01918	4·5	0·52329	0·00720
1·2	0·84269	−0·01104	4·8	0·47701	0·00738
1·5	0·94942	−0·00549	5·1	0·43482	0·00746
1·8	0·99600	−0·00144	5·4	0·39636	0·00747
2·1	0·99221	−0·00111	5·7	0·36130	0·00743
2·4	0·95270	−0·00270	6·0	0·32934	0·00733

TABLE 2. Real and imaginary parts of the eigenfunction for $R = 998$, $\beta = 0{\cdot}1122$.

Both Kurtz (1961) and Osborne in their time-amplified calculations have computed the eigenfunction for the same values of R and β. Their results agree very well so it is appropriate to consider a comparison with only one of them, say Kurtz.

This can be seen in figure 5 in which the real and imaginary parts of ϕ as obtained in the present work are shown in full lines for three Reynolds numbers including the one above. The points taken from Kurtz are plotted in each figure and should be compared with the curves labelled 3. The agreement between the two sets of results for Re ϕ is satisfactory but there are obvious differences between those for Im ϕ. Over the range $0 < z < 2$ the present results are more negative than the time-amplified ones by about 10 %, although over the remainder of the range both

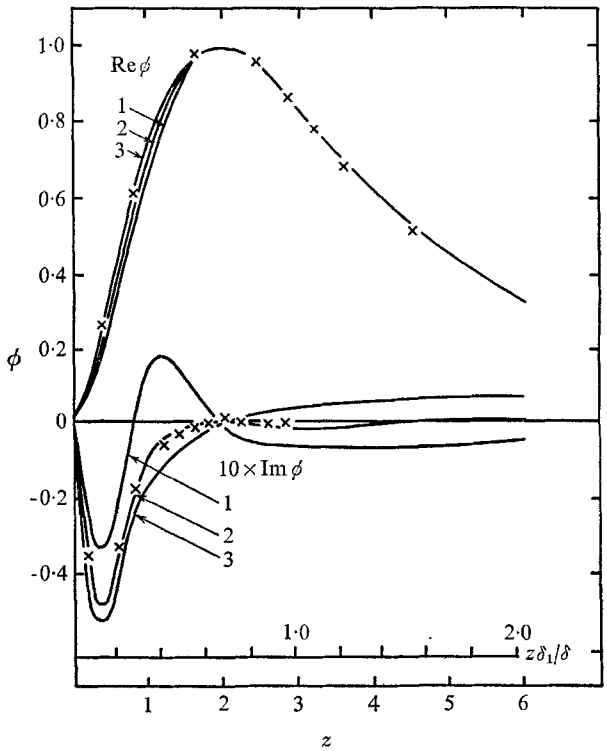

FIGURE 5. The eigenfunctions. Case 1, $R = 336$, $\beta = 0{\cdot}1297$, $\alpha_r = 0{\cdot}3084$, $\alpha_i = 0{\cdot}0079$. Case 2, $R = 598$, $\beta = 0{\cdot}1201$, $\alpha_r = 0{\cdot}3079$, $\alpha_i = -0{\cdot}0019$. Case 3, $R = 998$, $\beta = 0{\cdot}1122$, $\alpha_r = 0{\cdot}3086$, $\alpha_i = -0{\cdot}0057$. ×, points calculated for case 3 by Kurtz (1961).

sets of values are nearly zero. In fact Kurtz also gives distributions of ϕ for the values of R and β corresponding to curves 1 and 2; for the sake of clarity points from these distributions are not shown here. A further comparison at these two lower Reynolds numbers showed results similar to those just described, so it is possible that the differences over Im ϕ may be due to the intrinsic difference between time and space amplification.

In figure 6 the values of Re $d\phi/dz$ and Im $d\phi/dz$ are plotted against z for the same conditions as in figure 5. The agreement between the present results (curve 3) and those of Kurtz is better for the differentiated than the undifferentiated function. It is worth noting that the distribution of the r.m.s. amplitude of the x component of the perturbation velocity, which is proportional to $[(\text{Re}\, d\phi/dz)^2 + (\text{Im}\, d\phi/dz)^2]^{\frac{1}{2}}$ is given almost exactly by the plot of Re $d\phi/dz$

against z. As the Reynolds number increases the peak of this distribution moves closer to the plate which is in accordance with the experimental observations made at Edinburgh.

(v) *The distribution of Reynolds stress*

The component of Reynolds stress which is of chief interest is $-\overline{\rho uw}$ which interacts with the mean velocity gradient dU/dz to increase or decrease the energy of the perturbation. Thus if $-\overline{\rho uw}$ and dU/dz are of the same sign over a dominant part of the flow the perturbation grows in amplitude.

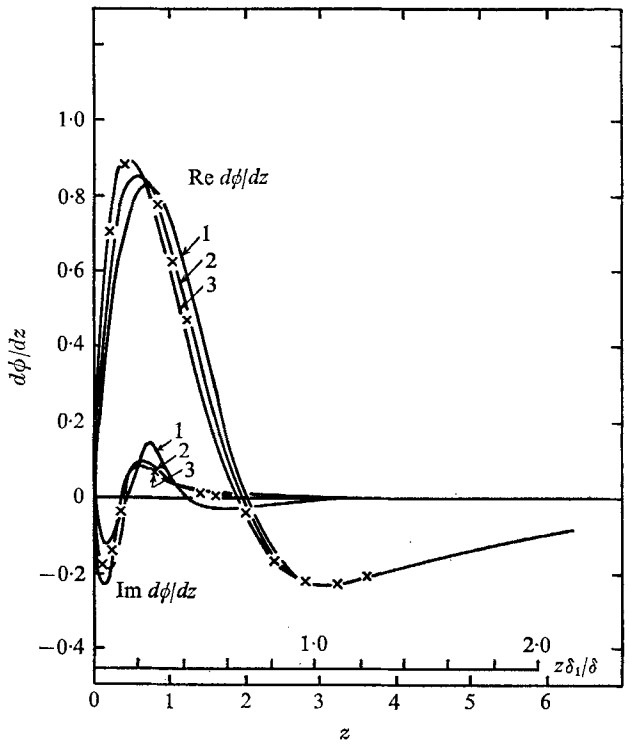

FIGURE 6. Derivatives of eigenfunctions. (Same conditions as figure 5.)

From the amplitude distributions given in the previous section, the Reynolds stress has been calculated using the formula

$$\overline{\rho uw} = \frac{1}{T}\int_0^T \rho uw\, dt, \tag{7}$$

where u and w are the instantaneous components of the perturbation velocity, parallel and perpendicular to the flat plate, and T is the period $2\pi/\beta$ of one oscillation. Taking $u = \mathrm{Re}\,\partial\psi/\partial z$ and $w = -\mathrm{Re}\,\partial\psi/\partial x$, where ψ is defined in (1), and substituting into the right-hand side of (7) then gives

$$-\overline{\rho uw} = \rho e^{-2\alpha_i x}[\alpha_r(\phi_r\phi_i' - \phi_r\phi_i) - \alpha_i(\phi_r\phi_r' + \phi_i\phi_i')].$$

$\phi_r(z)$ and $\phi_i(z)$ are the real and imaginary parts of the eigenfunction ϕ, and the primes indicate differentiation with respect to z. Since $e^{-2\alpha_i x}$ is independent of z,

it is convenient to omit it in the calculations and to define a Reynolds stress function S in the form

$$S = \alpha_r(\phi_r\phi_i' - \phi_r'\phi_i) - \alpha_i(\phi_r\phi_r' + \phi_i\phi_i').$$

This function is shown in figure 7 for the three cases considered in the last section. The curves show how the form of the Reynolds stress distribution varies with decreasing damping. Each distribution shows a peak close to the critical layer. In the damped case (labelled 1) the Reynolds stress then decreases rapidly and becomes quite strongly negative in the outer part of the boundary layer; in

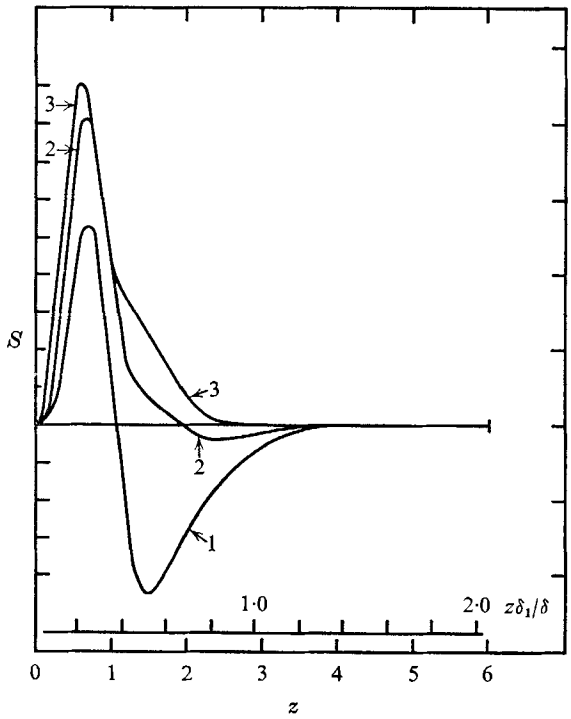

FIGURE 7. Distribution of Reynolds stress. (Same conditions as figure 5.)

case 2, slightly unstable, the Reynolds stress is much less negative in the outer part of the boundary layer, and in case 3, the Reynolds stress is positive over the whole range of z. The principal differences occur in the region between the critical layer and the outer edge of the boundary layer where for the unstable case energy is being transferred from the mean flow to the disturbance. This contrasts with the damped case where, in the outer part of the boundary layer the energy transfer is in the opposite direction. All three distributions show that the energy transfer is virtually restricted to the total thickness of the boundary layer.

The author wishes to thank Dr M. A. S. Ross and Mr D. Kershaw for their advice and encouragement in the course of the work described above. He also

acknowledges the great help given by the Edinburgh Regional Computing Centre on whose KDF 9 computer the calculations were carried out.

The work was assisted by a grant towards computing costs given by the Ministry of Technology.

REFERENCES

GASTER, M. 1962 *J. Fluid Mech.* **14**, 222.

GASTER, M. 1965 In *Progress in Aeronautical Science*, Vol. 6. Pergamon.

KAPLAN, R. E. 1964 ASRL-TR-116-1, *Cambridge Aerolastic and Structures Research Lab. Report M.I.T.* (STAR N64–29052).

KURTZ, E. F. 1961 Ph.D. Thesis, Dept of Mechanical Engineering M.I.T. (See also KURTZ, E. F. & CRANDALL, S. H. 1962 *J. Math. Phys.* **41**, 264.)

LIN, C. C. 1945 *Quart. Appl. Math.* **3**, 117, 218, 277.

NUMEROV, B. V. 1924 *Mon. Not. R. Astr. Soc.* **84**, 592.

OBREMSKI, H. J., MORKOVIN, M. V. & LANDAHL, M. 1969 AGARDograph 134, NATO, Paris.

OSBORNE, M. R. 1964 *Comput. J.* **7**, 3, 228.

OSBORNE, M. R. 1967 *SIAM J. Appl. Math.* **15**, 3, 539.

SCHLICHTING, H. 1935 *Nachr. Ges. Wiss. Göttingen. Math. Phys. Kl. Fachgruppe.* **1**, no. 4, 47–78.

SHEN, S. F. 1954 *J. Aero. Soc.* **21**, 62.

WAZZAN, A. R., OKAMURA, T. T. & SMITH, A. M. O. 1968 *Douglas Aircraft Company, Report* no. DAC–67086.